Inhibition of 12/15-Lipoxygenase Protects Against β-Cell Oxidative Stress and Glycemic Deterioration in Mouse Models of Type 1 Diabetes

Marimar Hernandez-Perez,[1] Gaurav Chopra,[2] Jonathan Fine,[2] Abass M. Conteh,[3] Ryan M. Anderson,[1,4] Amelia K. Linnemann,[1,3,4] Chanelle Benjamin,[1] Jennifer B. Nelson,[1] Kara S. Benninger,[1] Jerry L. Nadler,[5] David J. Maloney,[6] Sarah A. Tersey,[1] and Raghavendra G. Mirmira[1,3,4,7]

Diabetes 2017;66:2875–2887 | https://doi.org/10.2337/db17-0215

Islet β-cell dysfunction and aggressive macrophage activity are early features in the pathogenesis of type 1 diabetes (T1D). 12/15-Lipoxygenase (12/15-LOX) is induced in β-cells and macrophages during T1D and produces proinflammatory lipids and lipid peroxides that exacerbate β-cell dysfunction and macrophage activity. Inhibition of 12/15-LOX provides a potential therapeutic approach to prevent glycemic deterioration in T1D. Two inhibitors recently identified by our groups through screening efforts, ML127 and ML351, have been shown to selectively target 12/15-LOX with high potency. Only ML351 exhibited no apparent toxicity across a range of concentrations in mouse islets, and molecular modeling has suggested reduced promiscuity of ML351 compared with ML127. In mouse islets, incubation with ML351 improved glucose-stimulated insulin secretion in the presence of proinflammatory cytokines and triggered gene expression pathways responsive to oxidative stress and cell death. Consistent with a role for 12/15-LOX in promoting oxidative stress, its chemical inhibition reduced production of reactive oxygen species in both mouse and human islets in vitro. In a streptozotocin-induced model of T1D in mice, ML351 prevented the development of diabetes, with coincident enhancement of nuclear Nrf2 in islet cells, reduced β-cell oxidative stress, and preservation of β-cell mass. In the nonobese diabetic mouse model of T1D, administration of ML351 during the prediabetic phase prevented dysglycemia, reduced β-cell oxidative stress, and increased the proportion of anti-inflammatory macrophages in insulitis. The data provide the first evidence to date that small molecules that target 12/15-LOX can prevent progression of β-cell dysfunction and glycemic deterioration in models of T1D.

Diabetes is a disorder of glucose homeostasis that results from relative or absolute deficiency of insulin. In type 2 diabetes, a state of tissue insulin resistance prevails, and insulin-producing β-cells are unable to secrete sufficient insulin to overcome this resistance (1). By contrast, type 1 diabetes (T1D) is characterized by autoimmune-targeted destruction of β-cells, resulting in a state of absolute insulin deficiency (2). Whereas orally bioavailable small molecules have been developed and approved to prevent or treat type 2 diabetes, no such agents have been introduced to prevent or reverse the β-cell destruction seen in T1D. A challenge in the development of pharmacotherapies for T1D is the identification of specific pathways and targets that contribute to aggressive immune responses and/or β-cell death. Appreciation is increasing for oxidative stress and associated pathways within the β-cell that may predispose the β-cell to death upon activation of autoimmunity in T1D (3–5).

[1]Department of Pediatrics and the Center for Diabetes and Metabolic Diseases, Indiana University School of Medicine, Indianapolis, IN
[2]Department of Chemistry, Purdue Institute for Drug Discovery; Purdue Center for Cancer Research; Purdue Institute for Inflammation, Immunology and Infectious Disease; and Purdue Institute for Integrative Neuroscience, Purdue University, West Lafayette, IN
[3]Department of Biochemistry and Molecular Biology, Indiana University School of Medicine, Indianapolis, IN
[4]Department of Cellular and Integrative Physiology, Indiana University School of Medicine, Indianapolis, IN
[5]Department of Medicine, Eastern Virginia Medical School, Norfolk, VA
[6]National Center for Advancing Translational Sciences, National Institutes of Health, Rockville, MD
[7]Department of Medicine, Indiana University School of Medicine, Indianapolis, IN
Corresponding authors: Raghavendra G. Mirmira, rmirmira@iu.edu, and Sarah A. Tersey, stersey@iu.edu.

Received 21 February 2017 and accepted 15 August 2017.
This article contains Supplementary Data online at http://diabetes.diabetesjournals.org/lookup/suppl/doi:10.2337/db17-0215/-/DC1.

12/15-Lipoxygenase (12/15-LOX) is an enzyme encoded by the *Alox15* gene whose eicosanoid products contribute to inflammatory responses in macrophages and β-cells in the setting of diabetes (6). In mice, 12/15-LOX catalyzes the oxygenation of arachidonic acid at the 12 and 15 positions to form 12- and 15-hydroxyeicosatetraenoic acid (HETE), respectively, in an ~6:1 ratio (7). Global *Alox15*$^{-/-}$ mice are protected from diabetes in response to low-dose streptozotocin (STZ) (8), and *Alox15*$^{-/-}$ mice on the nonobese diabetic (NOD) background are protected from the development of T1D in this model (9). Despite a central role for the adaptive immune system in the inflammation associated with T1D, studies have suggested that the primary site of action of 12/15-LOX in conferring T1D risk may be in infiltrating macrophages and the β-cell itself, where it promotes oxidative and endoplasmic reticulum stress (10). Accordingly, we have shown that pancreas-specific *Alox15* knockout mice are protected from diabetes in the low-dose STZ model of T1D, raising the possibility that loss of 12/15-LOX in β-cells may be sufficient to prevent hyperglycemia in T1D, despite the continued presence of the enzyme in macrophages (11).

Apart from its role in T1D pathogenesis, 12/15-LOX and its lipid products (e.g., 12-HETE) have also been implicated in a variety of other inflammatory diseases, including obesity and insulin resistance (11–13), cardiovascular disease (14,15), and stroke (16,17), as well as in neurodegenerative diseases (18,19). Therefore, the development of specific 12/15-LOX inhibitors would have utility across a range of disorders. The absence of such specific and potent inhibitors of the LOX enzymes led members of our group to perform high-throughput screening to identify novel small-molecule inhibitors (20–23). Some of these inhibitors specifically protected β-cell lines and primary mouse and human islets from proinflammatory cytokine-induced dysfunction and death (24,25), but to date, none have been tested in models of diabetes in vivo. ML351 is a small-molecule inhibitor of 12/15-LOX with high potency and selectivity versus other LOX and cyclooxygenase enzymes (16,17). We sought to determine the efficacy of ML351 in models of T1D in vitro and in vivo, with a focus on its effects in islets.

RESEARCH DESIGN AND METHODS

Cells, Animals, and Assays

Mouse βTC3 β-cells were cultured and maintained as previously described (26). Mouse islets were isolated from collagenase-perfused pancreata as previously described (27), and human islets were obtained from the Integrated Islet Distribution Program. Cell cultures were treated with a cytokine cocktail containing 5 ng/mL interleukin-1β, 10 ng/mL tumor necrosis factor-α, and 100 ng/mL interferon-γ and/or with ML351 for 24 h. Caspase-3 activation assay was performed by using the Apo-ONE Homogeneous Caspase-3/7 Assay (Promega). Static glucose-stimulated insulin secretion (GSIS) assays and immunostaining for reactive oxygen species (ROS) with CellROX (Invitrogen) were performed as previously described (11).

Male C57BL/6J mice and female NOD/ShiLTJ (NOD) mice were purchased from The Jackson Laboratory. Female CD1 mice were purchased from Charles River Laboratories. Mice were maintained at the Indiana University vivarium according to protocols approved by the institutional animal care and use committee. Mice were injected intraperitoneally (IP) daily with ML351 dissolved in 80:17:3 PBS:cremophor:ethanol or vehicle alone. Glucose measurements and IP glucose tolerance tests (GTTs) were performed as described (28). Mice were euthanized, serum/pancreata harvested, and insulin measured as previously described (28).

Pharmacokinetic Analyses

ML351 was synthesized as described previously (23). ML351 was quantified in plasma and tissue by high-performance liquid chromatography-tandem mass spectrometry (AB SCIEX QTRAP 5500) by using temazepam as the internal standard. Pharmacokinetic parameters for ML351, including area under the curve (AUC) and $t_{1/2}$, were estimated by using noncompartmental methods. The maximum plasma concentration (C_{max}) and time of C_{max} (t_{max}) were obtained from the data. The AUC from 0 to infinity ($AUC_{0-\infty}$) was estimated from the AUC_{0-t} (time zero to the last quantifiable concentration [C_{last}]) and the AUC from C_{last} to infinity C_{last}/k_{el}, where k_{el} is the rate constant of elimination.

Immunohistochemistry and Immunofluorescence

Pancreata were fixed and immunostained as previously described (29) by using the antibodies indicated in Supplementary Table 1. 4-Hydroxynonenal (4-HNE) and glutathione peroxidase (GPX1) immunostainings were quantified by measuring pixel density per insulin-positive cell. Nrf2 was quantified by measuring nuclear and cytoplasmic pixel density per insulin-positive cell. Images were acquired with an LSM 700 confocal microscope (Zeiss). β-Cell mass and insulitis were calculated and scored from immunohistochemical staining as described previously (28,30) by using at least three pancreas sections 70 μm apart from five mice per group.

Docking of LOX Inhibitors to the Human Proteome

Fragment-based flexible docking method CANDOCK (31) was used to compute compound-proteome interaction signatures of the LOX inhibitors ML127 and ML351 with the human proteome, as done previously (31–34). Compound-proteome interaction scores of ML127 and ML351 were obtained with ~50% of the human proteome (14,595 human proteins) consisting of previously selected experimental and computationally modeled protein structures (31,33,34), where docking was done with only the flexibility of small molecules and not the proteins with default CANDOCK parameters. A total of 5,423 human proteins was also annotated into druggable protein classes (33) to predict toxicity of ML127 and ML351.

RNA Sequencing Analysis

RNA from treated islets (four biologic replicates per condition) was isolated with RNeasy Mini Kit (QIAGEN) and used to prepare a dual-indexed nonstranded cDNA library by using a SMART-Seq v4 Ultra Low Input RNA Kit

(Clontech). Libraries were sequenced with a HiSeq 4000 system (Illumina). All sequenced libraries were mapped to the mouse genome (University of California, Santa Cruz, Genome Browser assembly ID mm10) by using STAR RNA-seq aligner (35). The reads distribution across the genome was assessed by bamutils (from NGSUtils) (36). Uniquely mapped sequencing reads were assigned to mm10 refGene genes through featureCounts (from Subread) (37). Data were normalized by using the trimmed mean of M values method. Differential expression analysis was performed by DESeq2 (38). The Benjamini-Hochberg procedure was used to adjust *P* values for multiple hypothesis testing. For volcano plots, the fold change ($\log_2$ scale) differences in genes between groups were plotted on the *x*-axis, and the *P* values ($-\log_{10}$ scale) were plotted on the *y*-axis by using R (version 3.2) and the ggplot2 package (version 2.2.1). Gene ontology enrichments (enrichGO, Biological Processes) were performed by using the R package clusterProfiler (version 3.4.4, Bioconductor) (39).

Statistical Analysis

All data are presented as the mean ± SEM. One-way ANOVA (with Dunnett posttest) was used for comparisons involving more than two conditions, and a two-tailed Student *t* test was used for comparisons involving two conditions. Prism 7 software (GraphPad) was used for all statistical analyses. Statistical significance was assumed at $P < 0.05$.

RESULTS

Effects of LOX Inhibitors on Cell Viability

Several potent small-molecule inhibitors of human 12-LOX and 15-LOX enzymes were identified through quantitative high-throughput screening (20–22,24). Not previously tested was compound ML351, a mixed inhibitor that displayed nanomolar potency (IC_{50} ~200 nmol/L) against human 15-LOX (23). We first tested the effect of ML351 on cell apoptosis in mouse islets (Fig. 1*A*) and compared its effects with that of a related 12/15-LOX inhibitor, ML127 (Fig. 1*B*). As shown in Fig. 1*A* and *B*, ML351 displayed no deleterious effects on cellular apoptosis (by caspase activity assay) in the range between 1 and 50 μmol/L, whereas apoptosis was evident with ML127 at a concentration of 50 μmol/L (Fig. 1*B*). These studies suggest that ML127 exhibits greater cellular toxicity than ML351.

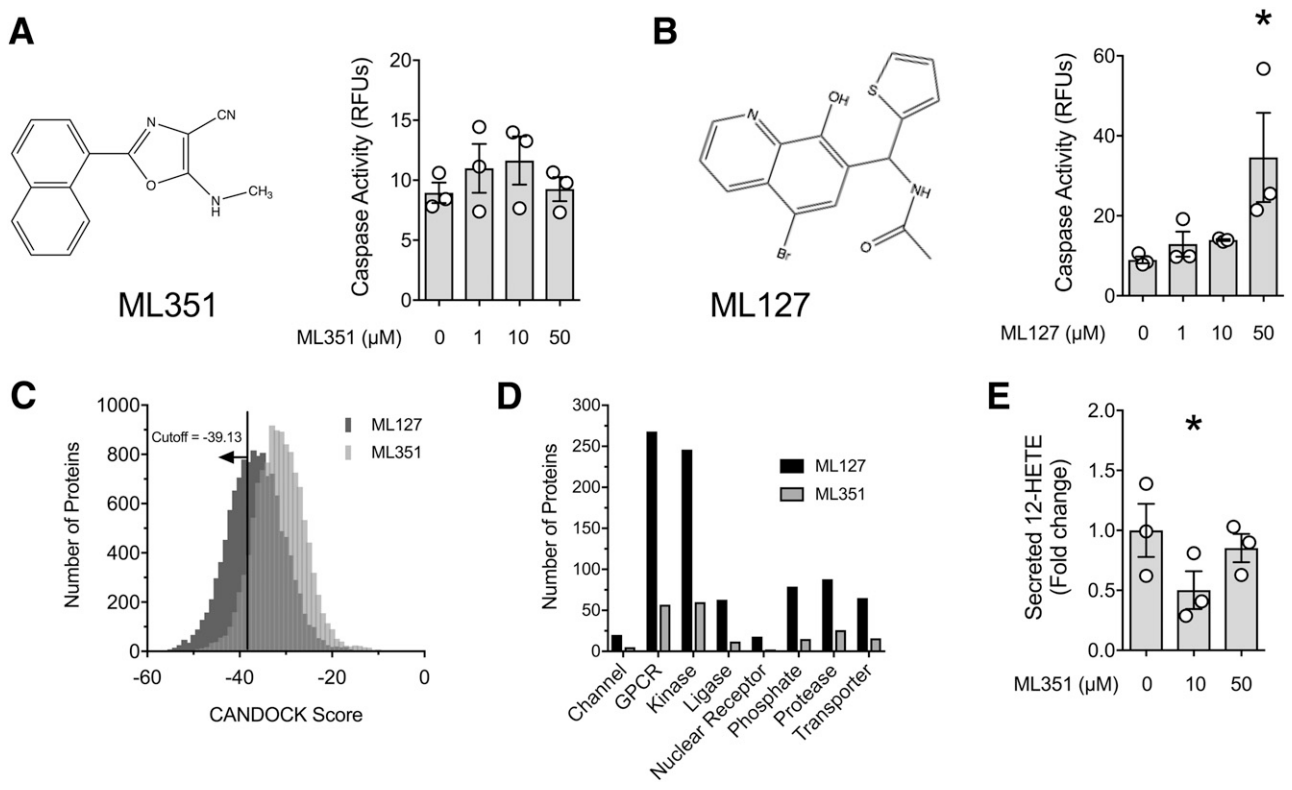

Figure 1—Toxicity of 12/15-LOX inhibitors in mouse islets. *A*: Chemical structure of ML351 and caspase activity measurements performed with mouse islets in the presence of varying doses of ML351 for 24 h. *B*: Chemical structure of ML127 and caspase activity measurements performed with mouse islets in the presence of varying doses of ML127 for 24 h. *C*: Distribution of CANDOCK scores with the number of human proteins predicted to bind to ML127 and ML351. Scores less than a cutoff of −39.13 are predicted strong binders for both compounds. *D*: Number of predicted strong binders for ML127 and ML351 distribution in eight druggable protein classes. *E*: 12-HETE levels in media from mouse islets incubated with the indicated concentrations of ML351 and proinflammatory cytokines for 4 h. Data are mean ± SEM ($n = 3$ independent experiments). *$P < 0.05$ for the comparisons indicated. GPCR, G-protein–coupled receptor; RFU, relative fluorescence unit.

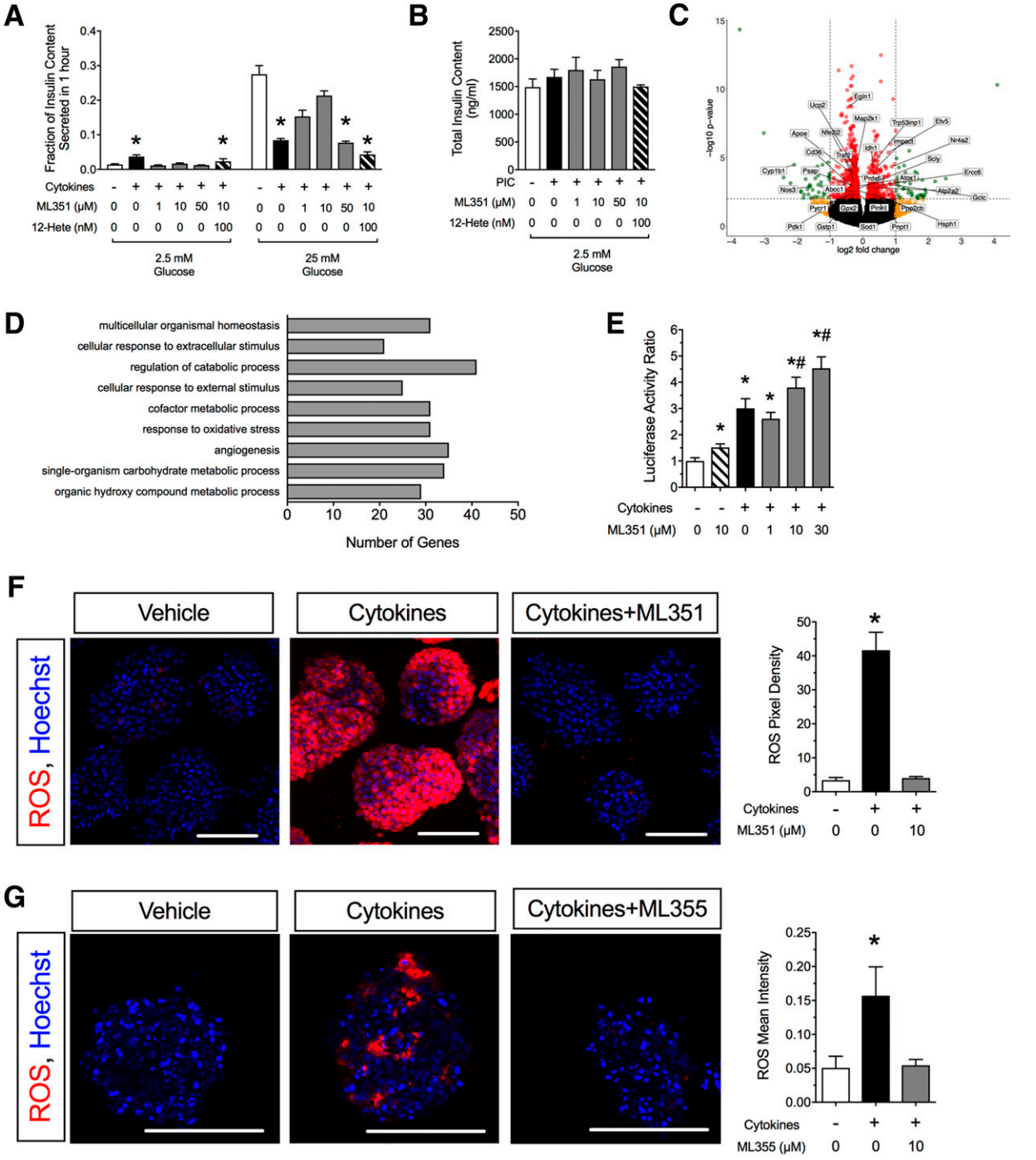

Figure 2—12/15-LOX inhibition protects against cytokine-induced islet dysfunction and oxidative stress. *A*: Mouse islets were incubated for 24 h with cytokines, ML351, and 12-HETE before exposure to low (2.5 mmol/L) and high (25 mmol/L) glucose, after which insulin levels in the medium were measured (n = 3–4 independent experiments). *P < 0.05 compared with control conditions (no cytokines, no ML351, no 12-HETE). *B*: Total islet insulin content for the insulin release experiments shown in *A*. *C*: Volcano plot of RNA sequencing analysis of mouse islets treated with cytokines + 10 μmol/L ML351 vs. cytokines alone for 24 h (n = 3 independent experiments; red, genes significantly altered [P < 0.05]; yellow, genes altered more than twofold; green, genes significantly altered more than twofold). *D*: Gene ontology pathway analysis of data shown in *C*. *E*: βTC3 β-cells were transfected with Nrf2-Luc reporter and incubated with ML351 at the concentrations indicated and then treated for 6 h with cytokine before luciferase activity measurement (n = 10 independent experiments). Data are luciferase activity normalized to control conditions (no cytokines, no ML351). *P < 0.05 compared with untreated control (no cytokines, no ML351). #P < 0.05 compared with cytokine treatment alone (no ML351). *F*: Mouse islets stained for ROS (CellROX reagent) (red) and DAPI (blue) upon treatment with or without cytokines and 10 μmol/L ML351. *G*: Human islets stained for ROS (CellROX reagent) (red) and DAPI (blue) upon treatment with or without cytokines and 10 μmol/L ML355. Original magnification ×200; scale bars = 100 μm. Bar graphs show quantitation of CellROX intensity in 10–16 islets from three independent mouse islet preparations (or human donors). *P < 0.05 compared with untreated islets (no cytokines, no ML compound). Data are mean ± SEM. PIC, proinflammatory cytokines.

Because toxicity often is related to off-target effects, we performed docking in silico of these inhibitors with ~50% of the human proteome (14,595 proteins). We restricted the analysis to the human proteome because comprehensive structural data for the mouse proteome are unavailable. As shown in Fig. 1*C*, ML127 has a significantly lower distribution of scores than ML351 (Kolmogorov-Smirnov test with $P < 2.2e\text{-}16$), suggesting that ML127 is a stronger interactor with non-LOX proteins (lower score = stronger interaction). By using a binding score of −39.13 (the score for the binding of ML127 to human 15-LOX, the ortholog of mouse 12/15-LOX) as a cutoff to predict off-target interactions, we identified 4,115 interacting proteins for ML127 and only 843 interacting proteins for ML351 (Supplementary Table 2 shows a complete list of scores). We separated the selected binders into druggable classes (channels, G-protein–coupled receptors, kinases, ligases, nuclear receptors, proteases, phosphatases, transporters). As shown in Fig. 1*D*, ML127 is predicted to bind to a substantially larger number of proteins than ML351, providing a possible explanation for its increased toxicity. We next tested the ability of ML351 to inhibit 12-HETE production in mouse islets. As shown in Fig. 1*E*, ML351 decreased 12-HETE release into islet medium at a dose of 10 μmol/L, but this effect was unexpectedly not observed at 50 μmol/L.

Effects and Mechanisms of ML351 on Cytokine-Induced Islet Dysfunction

To determine whether ML351 protects mouse islets in a T1D model in vitro, we performed coincubation experiments by using ML351 and proinflammatory cytokines (interleukin-1β, tumor necrosis factor-α, interferon-γ) (40) and measured GSIS. Compared with untreated islets, islets exposed to proinflammatory cytokines for 24 h exhibited increased insulin release at 2.5 mmol/L glucose (evidence of degranulation) and impaired insulin release in response to 25 mmol/L glucose (Fig. 2*A*). However, concurrent treatment with 10 μmol/L ML351 restored insulin secretion at 2.5 mmol/L glucose to control levels, and insulin release in response to 25 mmol/L glucose was significantly improved compared with treatment with proinflammatory cytokines alone (Fig. 2*A*). This protective effect can still be seen to a lesser extent with 1 μmol/L drug but is lost at 50 μmol/L (a dose at which no reduction in 12-HETE was observed) and when the effect of ML351 is bypassed by the addition of 100 nmol/L 12-HETE (Fig. 2*A*). The differences seen in GSIS assays were not caused by significant differences in total insulin content in islets (Fig. 2*B*).

To clarify the mechanism underlying the protective effects of ML351, we performed RNA sequencing analysis of islets treated with and without cytokines and with and without 10 μmol/L ML351. Principal component analysis showed distinct sample group clustering in the absence/presence of cytokines, with the addition of ML351 having less-pronounced effects than cytokines (Supplementary Fig. 1). When comparing the effect of ML351 in the presence of cytokines (by using false discovery rate <0.05 and fold change >2.0) (Fig. 2*C*), we found enrichment for genes corresponding to pathways responsive to extracellular signals, metabolism, and oxidative stress (Fig. 2*D*). Supplementary Table 3 lists all significantly altered genes.

Previously, we demonstrated that 12-HETE inhibits the nuclear translocation of the antioxidant transcription factor Nrf2 (11). As a readout of antioxidant activity in β-cells, we examined both an Nrf2 response element reporter in β-cell lines and ROS production in primary islets in response to ML351 treatment. As shown in Fig. 2*E*, when βTC3 cells transfected with the Nrf2 response element reporter were treated with 10 μmol/L ML351, no significant change in luciferase reporter activity was observed. When cells were treated with cytokines alone, a significant increase in luciferase activity was seen, which was increased further upon treatment with increasing doses of ML351 from 1 to 30 μmol/L. In accordance with the Nrf2 responses seen in the βTC3 cells, Fig. 2*F* shows that ML351 reversed the stimulation of ROS production in mouse islets in response to proinflammatory cytokines in vitro. A similar effect was observed in human islets treated with the human-specific 12-LOX inhibitor ML355 (Fig. 2*G*). Together, these results are consistent with an intracellular reduction in ROS in response to ML351 treatment.

Table 1—Pharmacokinetic properties of ML351 in C57BL/6J mice

Tissue	C_{max} (ng/mL or ng/g)*	t_{max} (h)	$AUC_{0-\infty}$ (ng/mL · h or ng/g · h)	$t_{1/2}$ (h)
IP injection				
Plasma	454	1	1,106	9.4
Brain	119	4	1,573	5.2
Fat	5,293	4	67,798	4.6
Liver	131	4	1,837	6.2
Pancreas	255	4	3,199	4.1
PO delivery				
Plasma	135	1	698	21.4
Brain	159	4	1,941	3.3
Fat	620	4	7,835	4.3
Liver	157	4	1,911	3.1
Pancreas	57	4	700	3.4

*Data units presented as nanograms per milliliter plasma or nanograms/gram tissue weight.

ML351 Protects Against STZ-Induced Diabetes in Mice

In pharmacokinetic studies in C57BL/6J mice, we analyzed the clearance of ML351 from the circulation tissues after IP and per os (PO) administration at 48 mg/kg (a dose previously used in mouse models of stroke) (16,17). Higher plasma and tissue levels (C_{max}) of ML351 were achieved after IP dosing than after PO dosing, and among the tissues analyzed (brain, fat, liver, pancreas), the drug preferentially distributed to fat (Table 1). Relatively greater distribution into pancreas was achieved after IP injection compared with PO delivery; therefore, we elected to pursue IP dosing for our models of diabetes in vivo.

We next asked whether ML351 protects against diabetes development in an STZ β-cell injury model that mimics the inflammation seen in T1D. C57BL/6J mice were administered five daily low doses of STZ, after which they were followed for the development of diabetes. In addition, mice were injected daily with a range of ML351 concentrations (0 [M0], 10 [M10], 24 [M24], or 48 [M48] mg/kg) starting 5 days before the beginning of the STZ series and concluding 5 days after the last dose of STZ (Fig. 3*A*). As shown in Fig. 3*B*, nanomolar levels of drug were measurable in plasma just before STZ; these levels directly correlated with the dosages administered. Animals that received STZ had significant reductions in weight compared with the no-STZ controls (Fig. 3*C*). However, at the end of the study, animals receiving STZ + M10 or STZ + M24 showed significantly less weight reduction than STZ + M0 animals; unexpectedly, the body weights of STZ + M48 animals resembled that of the STZ + M0 controls (Fig. 3*C*). Moreover, these two treatment groups (STZ + M0 and STZ + M48) exhibited frank hyperglycemia by day 9 of the study

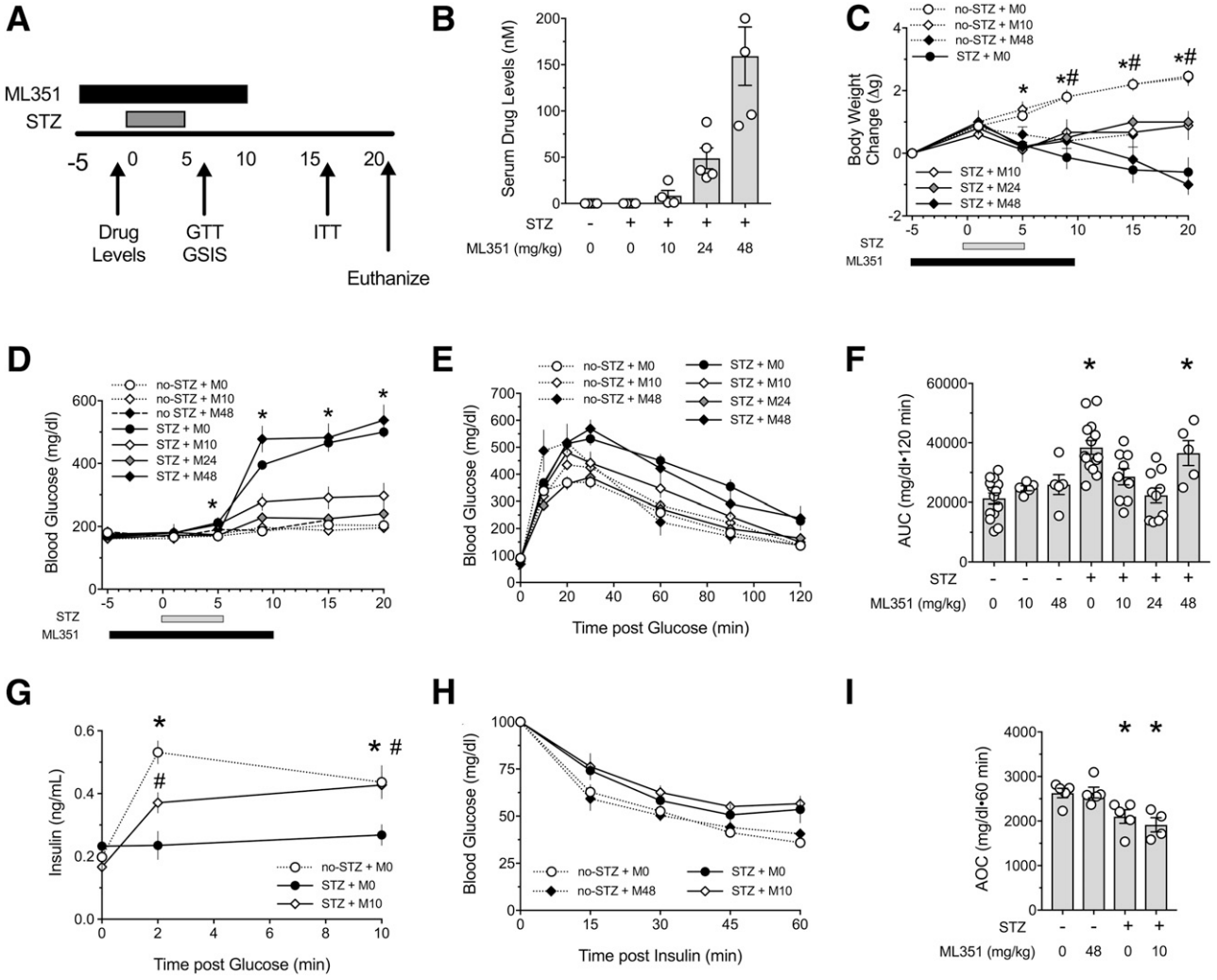

Figure 3—12/15-LOX inhibition protects against glycemic deterioration after multiple low-dose STZ injections. Nine-week-old male C57BL/6J mice were treated with vehicle or ML351. Multiple low-dose STZ injections (55 mg/kg) were given for 5 days (n = 5–15). *A*: Study design. *B*: Serum drug levels. *C*: Change in body weight from the start of the study. *D*: Random fed blood glucose measurements performed throughout the study. *E*: Results of GTTs performed at day 8. *F*: AUC from GTTs presented in *E*. *G*: GSIS in vivo. *H*: Results of ITTs performed at day 18. *I*: Area over the curve (AOC) from ITTs presented in *H*. Data are mean ± SEM. *$P < 0.05$ compared with no-STZ + M0. #$P < 0.05$ compared with STZ + M0.

(Fig. 3*D*) and significantly impaired GTTs (Fig. 3*E* and *F*). By contrast, animals administered STZ + M10 and STZ + M24 showed almost complete protection from hyperglycemia (Fig. 3*D*), and their GTTs were indistinguishable from animals not receiving STZ or animals receiving ML351 only (M10 or M48) (Fig. 3*E* and *F*). The improvement in glycemic control in the STZ + M10 animals was accompanied by improvements in GSIS in vivo (Fig. 3*G*). Although STZ treatment led to slight worsening of insulin tolerance compared with animals not receiving STZ, the addition of ML351 did not affect peripheral glucose utilization response to insulin in insulin tolerance tests (ITTs) (Fig. 3*H* and *I*).

ML351 Preserves β-Cell Mass and Attenuates STZ-Induced Oxidative Stress

As shown in representative images in Fig. 4*A*, islets of STZ + M0 and STZ + M48 animals were significantly reduced in size compared with non-STZ–treated controls, whereas STZ + M10 animals had islets that were indistinguishable from controls. Quantitative analysis of β-cell mass (Fig. 4*B*) demonstrated that the animals receiving STZ + M0 and STZ + M48 had statistically significantly reduced mass compared with non-STZ–treated controls, whereas animals in the STZ + M10 and STZ + M24 groups maintained statistically normal mass. Consistent with the β-cell mass findings, random insulin levels were reduced in the STZ + M0 and STZ + M48 groups compared with non-STZ–treated controls but were preserved in the animals receiving the lower doses of ML351 (Fig. 4*C*). Together, these data suggest that the lower doses of ML351 (10 and 24 mg/kg) protect β-cells from STZ.

The deleterious effects of 12-HETE are likely partly due to its inhibition of Nrf2-mediated transcription of antioxidant genes (11,41). We next immunostained pancreas tissues from STZ-treated and control animals for a marker of oxidative stress and for Nrf2. As shown in Fig. 5*A*, the remaining β-cells in mice treated with STZ + M0 exhibited a significant increase in 4-HNE staining, a marker of oxidative

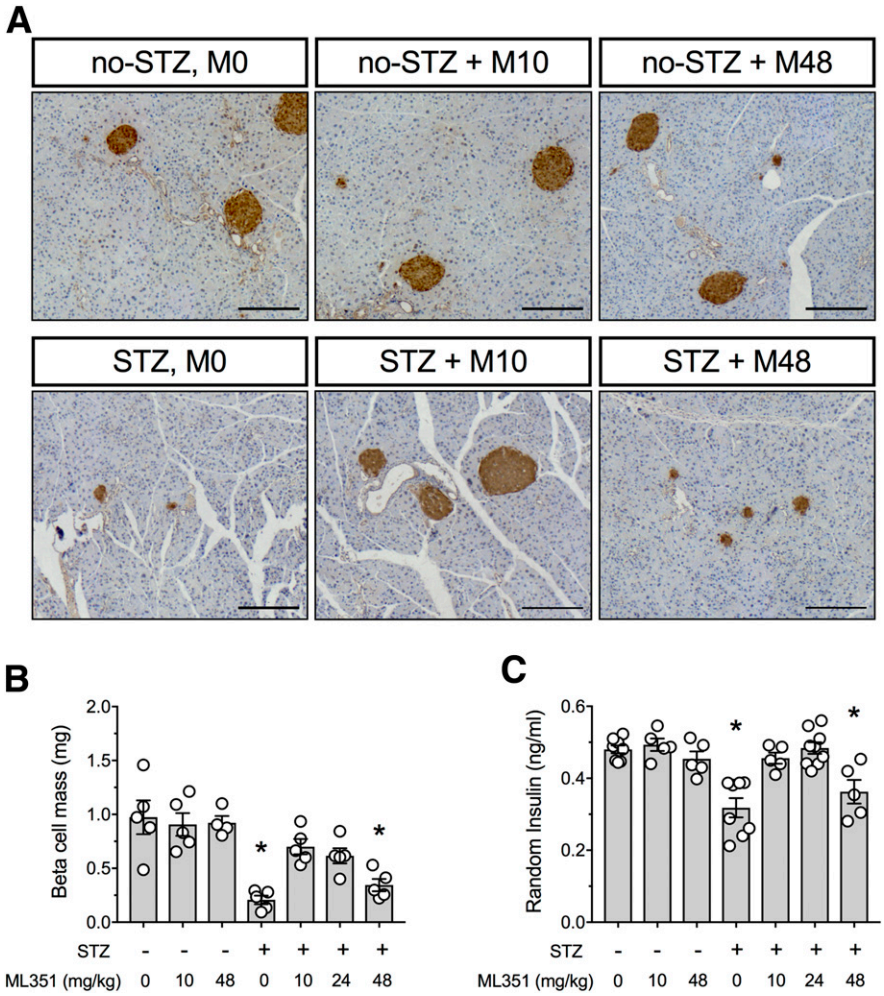

Figure 4—Effect of 12/15-LOX inhibition on β-cell mass and serum insulin in the multiple low-dose STZ diabetes mouse model. Nine-week-old male C57BL/6J mice were treated with vehicle or ML351. Multiple low-dose STZ injections (55 mg/kg) were given for 5 days (n = 5–15). *A*: Representative images of pancreata immunostained for insulin (brown) and counterstained for hematoxylin (blue). Original magnification ×100; scale bars = 200 μm. *B*: β-Cell mass of pancreata harvested at day 21. *C*: Random fed serum insulin levels. Data are mean ± SEM. *$P < 0.05$ compared with no-STZ + M0.

stress (11). In contrast, 4-HNE staining was reduced to control levels in STZ + M10 and STZ + M24 mice. The increased 4-HNE staining seen in STZ + M0 mice correlated with a statistically significant decrease in Nrf2 nuclear localization in β-cells, a finding that was slightly, but significantly, reversed in STZ + M10 and STZ + M24 mice (Fig. 5*B*). Immunostaining for GPX1, a target of Nrf2 activation, was accordingly decreased in β-cells of STZ + M0 mice but rescued to control levels in STZ + M24 and STZ + M10 mice (Fig. 5*C*).

ML351 Protects Against Early Glycemic Deterioration in NOD Mice

Female NOD mice develop spontaneous autoimmune diabetes between 12 and 24 weeks of age (5,30). A prelude to the development of diabetes in this model is β-cell dysfunction and consequent dysglycemia, which are evident as early as 6 weeks of age (5,42). To assess whether pharmacologic inhibition of 12/15-LOX protects against the early glycemic deterioration characteristic of this model, we administered 24 mg/kg of ML351 (M24) or vehicle (M0) by IP injection daily to female NOD mice beginning at 6 weeks of age for 2 weeks and then assessed glycemic control at 8 weeks of age; for comparison of the effects of the drug on a non-diabetes-prone strain, CD1 mice (an outbred strain closely related to NOD mice) were treated in parallel. Although fed blood glucose values at 8 weeks of age showed no differences between treated and untreated animals of either strain (Fig. 6*A*), GTTs showed that NOD + M24 animals exhibited improved glycemic control compared with NOD + M0 animals (Fig. 6*B* and *C*). CD1 + M0 and CD1 + M24 animals exhibited indistinguishable GTTs, suggesting that the drug had no effect on this strain (Fig. 6*B* and *C*). Analysis of pancreas from mice (Fig. 6*D*) revealed that β-cell mass was unaffected by administration of ML351 in either strain (Fig. 6*E*), signifying an effect of the drug on β-cell function in NOD animals. Consistent with improved β-cell function, a significant reduction in insulitis (Fig. 6*D*) and mean insulitis score (Fig. 6*F*) was observed in NOD + M24

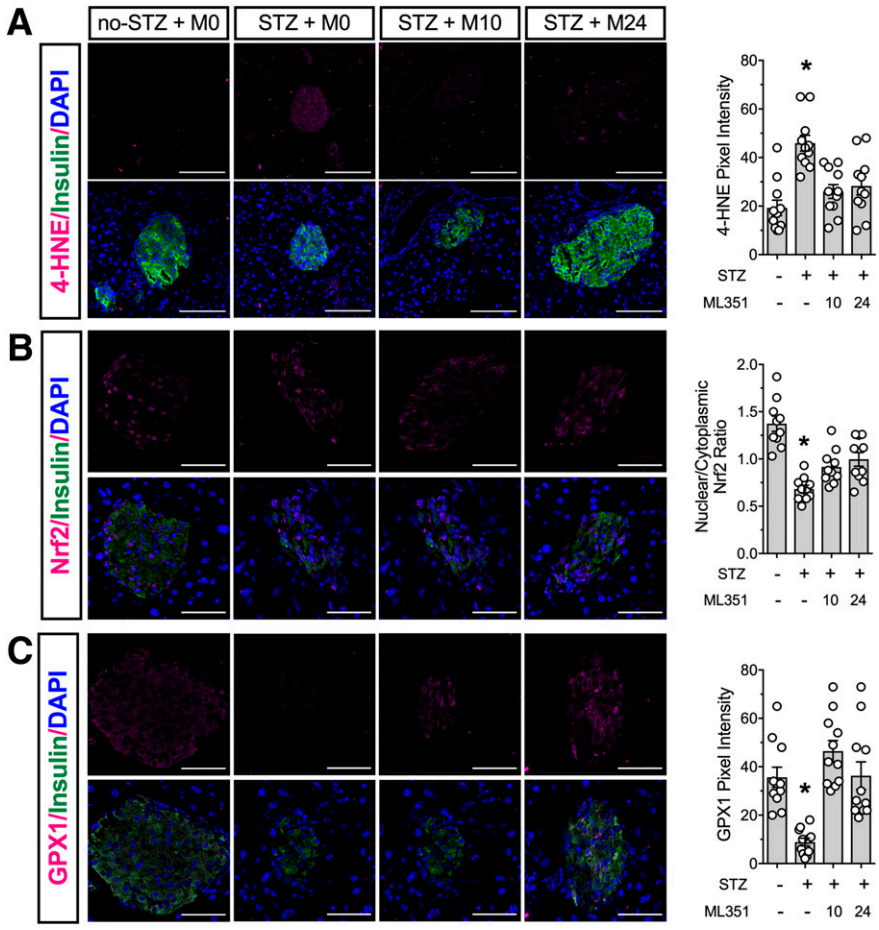

Figure 5—Inhibition of 12/15-LOX protects against islet oxidative stress in the multiple low-dose STZ diabetes mouse model. Nine-week-old male C57BL/6J mice were treated with vehicle or ML351. Multiple low-dose STZ injections (55 mg/kg) were given for 5 days (n = 5–15). Fixed pancreatic sections were subjected to immunofluorescence staining. Shown are representative images and the pixel density or nuclear/cytoplasmic ratio from analysis of at least three animals per group. *A*: Oxidative stress marker 4-HNE (magenta), insulin (green), and DAPI (blue). *B*: Nrf2 (magenta), insulin (green), and DAPI (blue). *C*: Antioxidant enzyme GPX1 (magenta), insulin (green), and DAPI (blue). Original magnification ×200; scale bars = 50 μm. *P < 0.05 compared with no-STZ + M0.

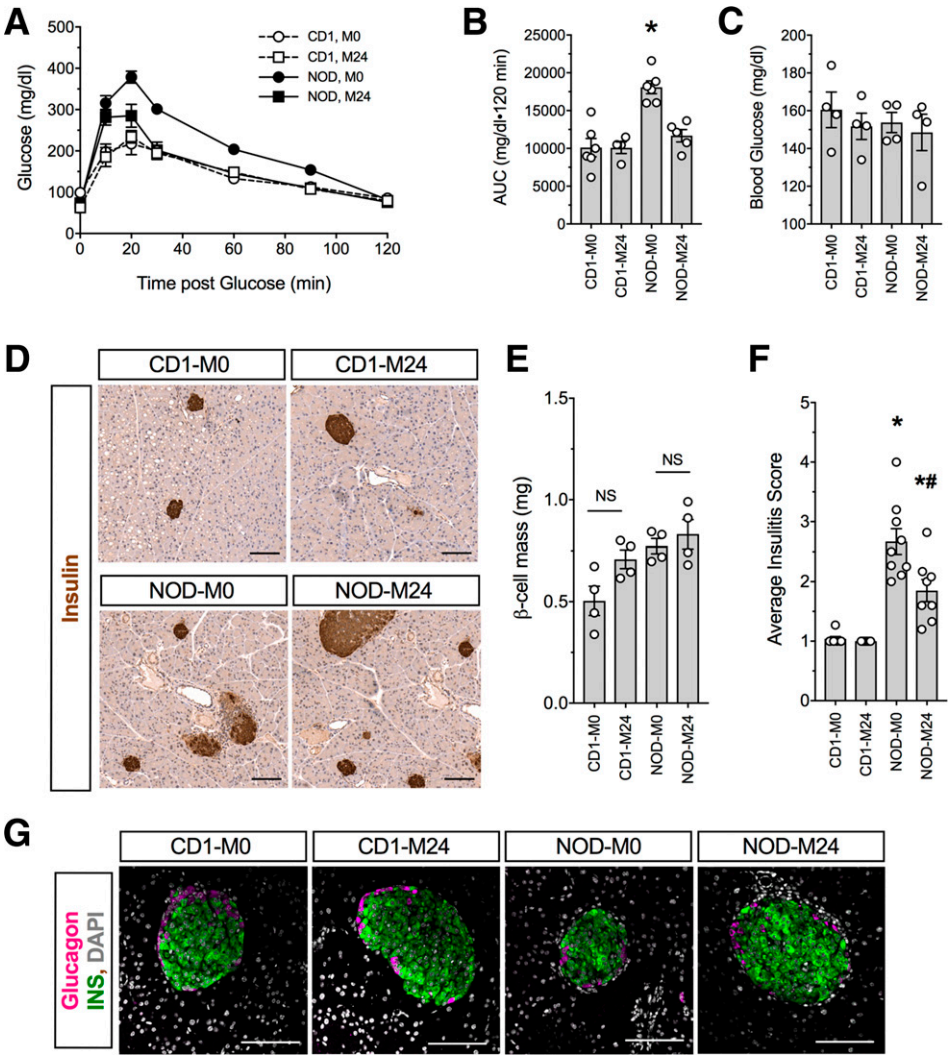

Figure 6—12/15-LOX inhibition mitigates glycemic deterioration in prediabetic NOD mice. Six-week-old NOD and CD1 female mice were injected daily for 2 weeks with vehicle or 24 mg/kg ML351 (n = 5). *A*: GTTs performed at 8 weeks of age. *B*: AUC of GTTs presented in *A*. *C*: Random fed blood glucose at 8 weeks of age. *D*: Representative images of pancreata immunostained for insulin (brown) and counterstained with hematoxylin (blue) from prediabetic 8-week-old mice. Original magnification ×100; scale bars = 100 μm. *E*: β-Cell mass of pancreata harvested at week 8. *F*: Average insulitis score. *G*: Representative images of pancreata immunostained for glucagon (magenta), insulin (green), and DAPI (gray). Original magnification ×200; scale bars = 100 μm. *P < 0.05 compared with CD1 + M0. #P < 0.05 compared with NOD + M0. INS, insulin; NS, not significant.

mice compared with NOD + M0 controls. Because insulitis is characterized by macrophages in early prediabetic NOD mice (43) and 12/15-LOX is also expressed in macrophages, we asked whether ML351 treatment affected the prevalence of anti-inflammatory, galectin 3–positive macrophages in the infiltrate (44). As shown in Supplementary Fig. 2, the insulitic infiltrate of NOD + M24 animals had a significantly greater percentage of galectin 3–positive macrophages than NOD + M0 animals.

Finally, we examined pancreatic tissue from CD1 and NOD mice for the presence of oxidative stress. β-Cells from NOD + M24 mice showed protection against oxidative stress (4-HNE staining) compared with NOD + M0 controls (Fig. 7*A*). This finding in NOD + M24 animals was consistent with increased β-cell Nrf2 nuclear localization (Fig. 7*B*) and increased GPX1 immunoreactivity (Fig. 7*C*) compared with NOD + M0 animals. ML351 had no effect on any of these parameters in CD1 mice (Fig. 7*A*–*C*).

DISCUSSION

The LOXs catalyze oxygenation of polyunsaturated fatty acids to form hydroperoxy fatty acids (e.g., 12-HETE) that generate ROS (45,46). In mice, 12/15-LOX, encoded by *Alox15*, contributes negatively to β-cell function (8,11,12,47,48), and the human 12-LOX enzyme levels are increased in islets of humans with T1D (49). Notwithstanding its potential role in T1D pathogenesis, no genetic variants of the LOX enzymes in humans have been closely linked to susceptibility for T1D (50). Nevertheless, given their pervasive roles in

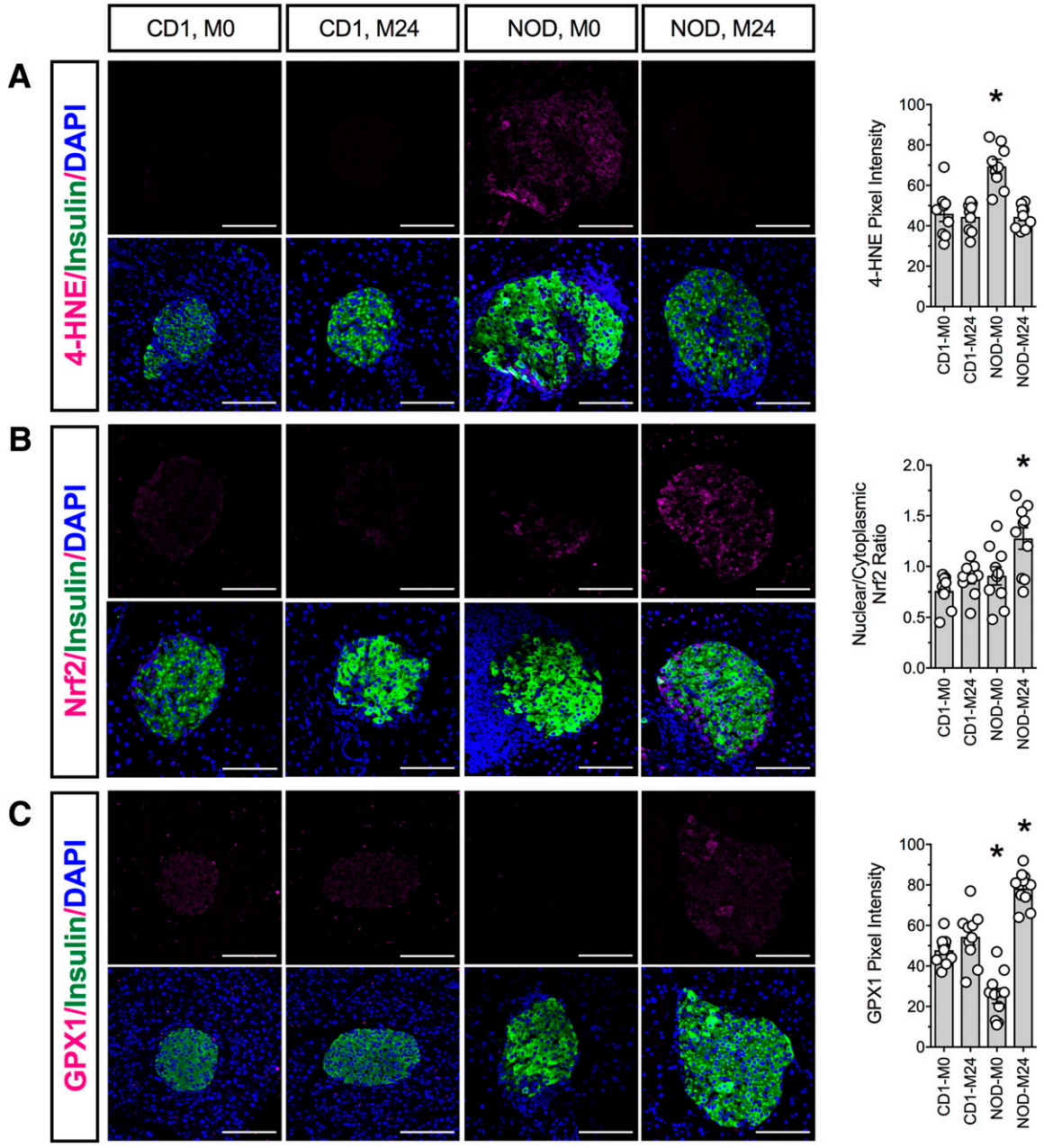

Figure 7—12/15-LOX inhibition reduces islet oxidative stress in prediabetic NOD mice. Fixed pancreatic sections from CD1 and NOD mice treated with vehicle or 24 mg/kg ML351 were subjected to immunofluorescence staining. Shown are representative images and the pixel density or nuclear/cytoplasmic ratio from analysis of at least three animals per group. *A*: Oxidative stress marker 4-HNE (magenta), insulin (green), and DAPI (blue). *B*: Nrf2 (magenta), insulin (green), and DAPI (blue). *C*: Antioxidant enzyme GPX1 (magenta), insulin (green), and DAPI (blue). Original magnification ×200; scale bars = 100 μm. *$P < 0.05$ compared with CD1 + M0.

many diseases, the LOXs have been prime targets for the development of small-molecule inhibitors. Early attempts to develop 12/15-LOX inhibitors met with limited success, with molecules lacking tight specificity, chemical tractability, or other drug-like properties. More recently, high-throughput screening of small-molecule drug libraries followed by chemical optimization have resulted in a series of compounds with nanomolar potency against 12/15-LOX (17,23,51). Studies of ML127 have shown promising results in blocking 12-HETE production in human and mouse islets (24). Here, we show that ML127 exhibits cytotoxicity at higher doses. By contrast, ML351 showed negligible cytotoxicity in vitro. These findings might be explained by off-target interactions, as predicted by computational docking to the human proteome. On the basis of these findings, we pursued ML351 as a prime candidate for 12/15-LOX inhibition in vitro and in vivo.

12-HETE functions as a proinflammatory lipid mediator (47,48) that increases cellular ROS either directly or through signaling through the putative receptor Gpr31 (52).

Consistent with inhibiting 12/15-LOX, ML351 exposure led to reduced 12-HETE release from mouse islets, reduced ROS generation in islets exposed to proinflammatory cytokines, and affected gene pathways involved in hypoxia, cellular death, and the antioxidant response. Although we did not see direct effects on genes involved in the endoplasmic reticulum stress pathway (a response that 12/15-LOX promotes [11,53]), these gene expression events likely occur later than the 24-h time point we examined in vitro (5).

To translate these studies to mouse models of diabetes, we performed pharmacokinetic studies and found that ML351 achieves penetrance in key metabolically active tissues after both IP and PO administration. We initially used a low-dose STZ mouse model of T1D in which low-level β-cell death induced by the alkylating effect of STZ leads to the influx of inflammatory cells (e.g., macrophages) and the subsequent local release of proinflammatory cytokines (28,54,55). In this context, the current studies show that ML351 prevents β-cell oxidative stress, β-cell dysfunction, and hyperglycemia in treated mice. Of note, a higher dose of ML351 (48 mg/kg) had no protective effect. Although this finding indicates an independent toxic effect of ML351 at higher doses, this seems unlikely because the mice treated with 48 mg/kg alone showed normoglycemia. The current studies of ML351 in vitro, wherein higher doses of the drug (50 μmol/L) failed to inhibit 12-HETE production or reverse cytokine effects on GSIS, raise the likely possibility that aggressive inhibition of 12/15-LOX at high doses of ML351 causes compensatory activity of another LOX isoform (12-LOX) to generate 12-HETE.

In prior studies, we showed an effect of 12-HETE in inhibiting the nuclear translocation of Nrf2, thereby preventing its consequent transcription of genes encoding antioxidant enzymes (11). We show in the current study that ML351 also enhances activity of an Nrf2 reporter in cell lines and promotes nuclear translocation of Nrf2 and activation of GPX1 in β-cells of STZ-treated mice. Given the similarity of these pharmacologic studies to our earlier pancreas-specific knockout studies of *Alox15* (11), ML351 possibly inhibited 12/15-LOX directly in β-cells. However, we cannot rule out that inhibition of 12/15-LOX in macrophages may have also contributed to the β-cell–protective effect in this model. Given the relative scarcity of macrophage infiltration in the STZ model (54), quantitative assessment of the effects of ML351 on macrophages is difficult. In this regard, the NOD model provides more insight. Treatment of NOD mice with ML351 led to improved glycemic control and significantly reduced insulitis. The reduction of β-cell death in NOD mice has been suggested to lead to reductions in insulitis, likely by mitigating the chemotactic signals released by dying β-cells (4,5). On the other hand, we observed that galectin 3–positive anti-inflammatory macrophages make up a greater percentage of the insulitic infiltrate, which points to a possible direct effect of the drug on macrophages. In this regard, ROS has been proposed as an important mediator of immune cell pathogenicity that allows for initiation and propagation of insulitis (56). Treatment with ML351, therefore, may mitigate insulitis by reducing ROS production in innate and adaptive immune cells.

Although this study is an important first step toward the translation of a new drug class for the prevention of diabetes, significant hurdles remain. Whereas the LOXs are structurally homologous between mice and humans, differences in function and spatial expression of LOXs exist between the species. As noted, the LOX encoded by *Alox15* is the primary LOX expressed in mouse β-cells and macrophages, whereas in humans this LOX is encoded by *ALOX12*. In biochemical studies, ML351 demonstrated >250-fold selectivity for the human LOX encoded by *ALOX15* versus *ALOX12* (23). As such, ML351 would not be an ideal choice for targeting the relevant LOX in human β-cells and macrophages. Conversely, a related drug, ML355, exhibits selectivity for human LOX encoded by *ALOX12* (21,25) and appears to have similar effects on reducing human islet ROS production (shown here). Unfortunately, ML355 cannot as yet be tested in preclinical models in vivo. This limitation to preclinical testing must await either the selection of a better model organism or the humanization of the mouse *Alox15* alleles. In the meantime, the studies presented here offer an important new insight into the feasibility of inhibiting 12/15-LOX for the prevention and treatment of T1D.

Acknowledgments. The authors thank A. Acton of the Indiana University Center for Diabetes and Metabolic Diseases Translation Core laboratories for expert assistance in insulin measurements and the Islet Core for the isolation of islets and metabolic characterization of mice. The authors also thank S. Nakshatri at Indiana University for assistance in immunostaining and T. Holman at the University of California, Santa Cruz for valuable discussion.

Funding. This work was supported by National Institute of Diabetes and Digestive and Kidney Diseases (NIDDK) grants T32-DK-064466 (to M.H.-P. and C.B.) and R01-DK-105588 (to J.L.N. and R.G.M.) This study used Diabetes Center core resources supported by NIDDK grant P30-DK-097512 (to R.G.M.). G.C. acknowledges support from Purdue University start-up funds. Additional analytical work was performed by the Clinical Pharmacology Analytical Core laboratory of the Indiana University Melvin and Bren Simon Cancer Center supported by National Cancer Institute grant P30-CA-082709. Microarray studies were carried out in the Center for Medical Genomics at Indiana University School of Medicine, which is partially supported by the Indiana Genomic Initiative at Indiana University (INGEN); INGEN is supported in part by the Lilly Endowment, Inc.

Duality of Interest. No potential conflicts of interest relevant to this article were reported.

Author Contributions. M.H.-P., G.C., J.F., and S.A.T. designed experiments, performed research, contributed to the discussion, and wrote the manuscript. J.F., A.M.C., C.B., J.B.N., and K.S.B. performed research and contributed to the discussion. R.M.A. and R.G.M. designed experiments, contributed to the discussion, and wrote the manuscript. A.K.L., J.L.N., and D.J.M. designed experiments, provided reagents, and contributed to the discussion. All authors reviewed and concurred with the final manuscript. M.H.-P., S.A.T., and R.G.M. are the guarantors of this work and, as such, had full access to all the data in the study and take responsibility for the integrity of the data and the accuracy of the data analysis.

Prior Presentation. Parts of this study were presented in abstract form at the 77th Scientific Sessions of the American Diabetes Association, San Diego, CA, 9–13 June 2017.

References

1. Ogihara T, Mirmira RG. An islet in distress: β cell failure in type 2 diabetes. J Diabetes Investig 2010;1:123–133
2. Eizirik DL, Colli ML, Ortis F. The role of inflammation in insulitis and beta-cell loss in type 1 diabetes. Nat Rev Endocrinol 2009;5:219–226
3. Delmastro MM, Piganelli JD. Oxidative stress and redox modulation potential in type 1 diabetes. Clin Dev Immunol 2011;2011:593863
4. Maganti AV, Tersey SA, Syed F, et al. Peroxisome proliferator-activated receptor-γ activation augments the β-cell unfolded protein response and rescues early glycemic deterioration and β cell death in non-obese diabetic mice. J Biol Chem 2016;291:22524–22533
5. Tersey SA, Nishiki Y, Templin AT, et al. Islet β-cell endoplasmic reticulum stress precedes the onset of type 1 diabetes in the nonobese diabetic mouse model. Diabetes 2012;61:818–827
6. Tersey SA, Bolanis E, Holman TR, Maloney DJ, Nadler JL, Mirmira RG. Minireview: 12-lipoxygenase and islet β-cell dysfunction in diabetes. Mol Endocrinol 2015;29:791–800
7. Haeggström JZ, Funk CD. Lipoxygenase and leukotriene pathways: biochemistry, biology, and roles in disease. Chem Rev 2011;111:5866–5898
8. Bleich D, Chen S, Zipser B, Sun D, Funk CD, Nadler JL. Resistance to type 1 diabetes induction in 12-lipoxygenase knockout mice. J Clin Invest 1999;103:1431–1436
9. McDuffie M, Maybee NA, Keller SR, et al. Nonobese diabetic (NOD) mice congenic for a targeted deletion of 12/15-lipoxygenase are protected from autoimmune diabetes. Diabetes 2008;57:199–208
10. Green-Mitchell SM, Tersey SA, Cole BK, et al. Deletion of 12/15-lipoxygenase alters macrophage and islet function in NOD-Alox15(null) mice, leading to protection against type 1 diabetes development. PLoS One 2013;8:e56763
11. Tersey SA, Maier B, Nishiki Y, Maganti AV, Nadler JL, Mirmira RG. 12-lipoxygenase promotes obesity-induced oxidative stress in pancreatic islets. Mol Cell Biol 2014;34:3735–3745
12. Nunemaker CS, Chen M, Pei H, et al. 12-Lipoxygenase-knockout mice are resistant to inflammatory effects of obesity induced by western diet. Am J Physiol Endocrinol Metab 2008;295:E1065–E1075
13. Sears DD, Miles PD, Chapman J, et al. 12/15-Lipoxygenase is required for the early onset of high fat diet-induced adipose tissue inflammation and insulin resistance in mice. PLoS One 2009;4:e7250
14. Cyrus T, Witztum JL, Rader DJ, et al. Disruption of the 12/15-lipoxygenase gene diminishes atherosclerosis in apo E-deficient mice. J Clin Invest 1999;103:1597–1604
15. George J, Afek A, Shaish A, et al. 12/15-Lipoxygenase gene disruption attenuates atherogenesis in LDL receptor-deficient mice. Circulation 2001;104:1646–1650
16. Liu Y, Zheng Y, Karatas H, et al. 12/15-Lipoxygenase inhibition or knockout reduces warfarin-associated hemorrhagic transformation after experimental stroke. Stroke 2017;48:445–451
17. Rai G, Joshi N, Jung JE, et al. Potent and selective inhibitors of human reticulocyte 12/15-lipoxygenase as anti-stroke therapies. J Med Chem 2014;57:4035–4048
18. Chu J, Li J-G, Giannopoulos PF, et al. Pharmacologic blockade of 12/15-lipoxygenase ameliorates memory deficits, Aβ and tau neuropathology in the triple-transgenic mice. Mol Psychiatry 2015;20:1329–1338
19. Yang H, Zhuo J-M, Chu J, Chinnici C, Praticò D. Amelioration of the Alzheimer's disease phenotype by absence of 12/15-lipoxygenase. Biol Psychiatry 2010;68:922–929
20. Kenyon V, Rai G, Jadhav A, et al. Discovery of potent and selective inhibitors of human platelet-type 12- lipoxygenase. J Med Chem 2011;54:5485–5497
21. Luci D, Jameson JB II, Yasgar A, et al. Discovery of ML355, a potent and selective inhibitor of human 12-lipoxygenase. Available from http://www.ncbi.nlm.nih.gov/books/NBK259188. Accessed 24 January 2015
22. Luci DK, Jameson JB 2nd, Yasgar A, et al. Synthesis and structure-activity relationship studies of 4-((2-hydroxy-3-methoxybenzyl)amino)benzenesulfonamide derivatives as potent and selective inhibitors of 12-lipoxygenase. J Med Chem 2014;57:495–506
23. Rai G, Joshi N, Perry S, et al. Discovery of ML351, a potent and selective inhibitor of human 15-lipoxygenase-1. Available from http://www.ncbi.nlm.nih.gov/books/NBK190602. Accessed 4 July 2014
24. Taylor-Fishwick DA, Weaver J, Glenn L, et al. Selective inhibition of 12-lipoxygenase protects islets and beta cells from inflammatory cytokine-mediated beta cell dysfunction. Diabetologia 2015;58:549–557
25. Ma K, Park SH, Lindsey G, et al. 12-lipoxygenase inhibitor improves functions of cytokine-treated human islets and type 2 diabetic islets. J Clin Endocrinol Metab 2017;102:2789–2797
26. Chakrabarti SK, James JC, Mirmira RG. Quantitative assessment of gene targeting in vitro and in vivo by the pancreatic transcription factor, Pdx1. Importance of chromatin structure in directing promoter binding. J Biol Chem 2002;277:13286–13293
27. Stull ND, Breite A, McCarthy R, Tersey SA, Mirmira RG. Mouse islet of Langerhans isolation using a combination of purified collagenase and neutral protease. J Vis Exp 2012;67:e4137
28. Maier B, Ogihara T, Trace AP, et al. The unique hypusine modification of eIF5A promotes islet beta cell inflammation and dysfunction in mice. J Clin Invest 2010;120:2156–2170
29. Evans-Molina C, Robbins RD, Kono T, et al. Peroxisome proliferator-activated receptor gamma activation restores islet function in diabetic mice through reduction of endoplasmic reticulum stress and maintenance of euchromatin structure. Mol Cell Biol 2009;29:2053–2067
30. Cabrera SM, Colvin SC, Tersey SA, Maier B, Nadler JL, Mirmira RG. Effects of combination therapy with dipeptidyl peptidase-IV and histone deacetylase inhibitors in the non-obese diabetic mouse model of type 1 diabetes. Clin Exp Immunol 2013;172:375–382
31. Chopra G, Samudrala R. Exploring polypharmacology in drug discovery and repurposing using the CANDO platform. Curr Pharm Des 2016;22:3109–3123
32. Chopra G, Kaushik S, Elkin PL, Samudrala R. Combating ebola with repurposed therapeutics using the CANDO platform. Molecules 2016;21:E1537
33. Sethi G, Chopra G, Samudrala R. Multiscale modelling of relationships between protein classes and drug behavior across all diseases using the CANDO platform. Mini Rev Med Chem 2015;15:705–717
34. Minie M, Chopra G, Sethi G, et al. CANDO and the infinite drug discovery frontier. Drug Discov Today 2014;19:1353–1363
35. Dobin A, Davis CA, Schlesinger F, et al. STAR: ultrafast universal RNA-seq aligner. Bioinformatics 2013;29:15–21
36. Breese MR, Liu Y. NGSUtils: a software suite for analyzing and manipulating next-generation sequencing datasets. Bioinformatics 2013;29:494–496
37. Liao Y, Smyth GK, Shi W. featureCounts: an efficient general purpose program for assigning sequence reads to genomic features. Bioinformatics 2014;30:923–930
38. Love MI, Huber W, Anders S. Moderated estimation of fold change and dispersion for RNA-seq data with DESeq2. Genome Biol 2014;15:550
39. Yu G, Wang L-G, Han Y, He Q-Y. clusterProfiler: an R package for comparing biological themes among gene clusters. OMICS 2012;16:284–287
40. Jörns A, Arndt T, Meyer zu Vilsendorf A, et al. Islet infiltration, cytokine expression and β cell death in the NOD mouse, BB rat, Komeda rat, LEW.1AR1-iddm rat and humans with type 1 diabetes. Diabetologia 2014;57:512–521
41. Yeh C-H, Ma K-H, Liu P-S, Kuo J-K, Chueh S-H. Baicalein decreases hydrogen peroxide-induced damage to NG108-15 cells via upregulation of Nrf2. J Cell Physiol 2015;230:1840–1851
42. Ize-Ludlow D, Lightfoot YL, Parker M, et al. Progressive erosion of β-cell function precedes the onset of hyperglycemia in the NOD mouse model of type 1 diabetes. Diabetes 2011;60:2086–2091
43. Charré S, Rosmalen JGM, Pelegri C, et al. Abnormalities in dendritic cell and macrophage accumulation in the pancreas of nonobese diabetic (NOD) mice during the early neonatal period. Histol Histopathol 2002;17:393–401
44. MacKinnon AC, Farnworth SL, Hodkinson PS, et al. Regulation of alternative macrophage activation by galectin-3. J Immunol 2008;180:2650–2658

45. Brash AR. Lipoxygenases: occurrence, functions, catalysis, and acquisition of substrate. J Biol Chem 1999;274:23679–23682
46. Solomon EI, Zhou J, Neese F, Pavel EG. New insights from spectroscopy into the structure/function relationships of lipoxygenases. Chem Biol 1997;4:795–808
47. Chen M, Yang ZD, Smith KM, Carter JD, Nadler JL. Activation of 12-lipoxygenase in proinflammatory cytokine-mediated beta cell toxicity. Diabetologia 2005;48:486–495
48. Ma K, Nunemaker CS, Wu R, Chakrabarti SK, Taylor-Fishwick DA, Nadler JL. 12-lipoxygenase products reduce insulin secretion and beta-cell viability in human islets. J Clin Endocrinol Metab 2010;95:887–893
49. Grzesik WJ, Nadler JL, Machida Y, Nadler JL, Imai Y, Morris MA. Expression pattern of 12-lipoxygenase in human islets with type 1 diabetes and type 2 diabetes. J Clin Endocrinol Metab 2015;100:E387–E395
50. Ram R, Mehta M, Nguyen QT, et al. Systematic evaluation of genes and genetic variants associated with type 1 diabetes susceptibility. J Immunol 2016;196:3043–3053
51. Rai G, Kenyon V, Jadhav A, et al. Discovery of potent and selective inhibitors of human reticulocyte 15-lipoxygenase-1. J Med Chem 2010;53:7392–7404
52. Guo Y, Zhang W, Giroux C, et al. Identification of the orphan G protein-coupled receptor GPR31 as a receptor for 12-(S)-hydroxyeicosatetraenoic acid. J Biol Chem 2011;286:33832–33840
53. Cole BK, Kuhn NS, Green-Mitchell SM, et al. 12/15-Lipoxygenase signaling in the endoplasmic reticulum stress response. Am J Physiol Endocrinol Metab 2012; 302:E654–E665
54. Calderon B, Suri A, Miller MJ, Unanue ER. Dendritic cells in islets of Langerhans constitutively present beta cell-derived peptides bound to their class II MHC molecules. Proc Natl Acad Sci U S A 2008;105:6121–6126
55. Lukić ML, Stosić-Grujicić S, Shahin A. Effector mechanisms in low-dose streptozotocin-induced diabetes. Dev Immunol 1998;6:119–128
56. Padgett LE, Broniowska KA, Hansen PA, Corbett JA, Tse HM. The role of reactive oxygen species and proinflammatory cytokines in type 1 diabetes pathogenesis. Ann N Y Acad Sci 2013;1281:16–35